*Machine Copy for Proofreading, Vol. x, y–z, 2009*

# MAGNETIC FIELD IN MRI YOKELESS DEVICES: ANALYTICAL APPROACH

**R. Ravaud and G. Lemarquand**

Laboratoire d'Acoustique de l'Universite du Maine,
UMR CNRS 6613, Avenue Olivier Messiaen, 72085 Le Mans, France
guy.lemarquand@univ-lemans.fr

**Abstract**—This paper presents a three-dimensional analytical expressions for studying the static magnetic field produced by Magnetic Resonance Imaging structures. This medical imaging technique uses a very high and uniform magnetic field produced by ring permanent magnets with rotating polarizations. However, the manufacturing of such ring permanent magnets is difficult to realize. Consequently, such ring permanent magnets are replaced by assemblies of tile permanent magnets uniformly magnetized. Unfortunately, the magnetic field produced by these tile permanent magnets uniformly magnetized is both less important and less uniform than the one produced by an idealized ring permanent magnet. We propose in this paper to study the influence of the number of tile permanent magnets used on the magnetic field properties.

## 1. INTRODUCTION

Magnetic Resonance Imaging is a medical imaging technique widely used in radiology to visualize the internal structure of a body. This technique generally uses a very high static magnetic field produced by permanent magnets [1]-[4]. It is well known that the magnetic field homogeneity of imaging region is the most important criterion for optimizing MRI structures [5][6]. On the other hand, the magnetic field must be the greatest [7]-[9].
Several approaches have been carried out for optimizing MRI structures so as to improve the magnetic field homogeneity as well as its magnitude [10][11]. Strictly speaking, these approaches are based on either analytical [12] or numerical approaches [13]. For example, the finite-element method has been used for studying MRI devices made of permanent magnets [14]. Furthermore, some original methods have been proposed for designing MRI structures made of

permanent magnets [15] by employing inverse methods [16]. All these studies deal with the optimization of the static field produced by permanent magnets or currents in coils. In the case of MRI made of permanent magnets, this static magnetic field is generated by tile permanent magnets with uniform polarizations [17][18]. However, most of the studies dealing with the magnetic field produced by MRI structures assume that the magnetic field is produced by a ring permanent magnet with a rotating polarization. However, this is not the case in practice because it is very difficult to manufacturate such ring permanent magnets. Consequently, the ring permanent magnet generating the magnetic field is replaced by an assembly of tile permanent magnets uniformly magnetized. As a consequence, the magnetic field magnitude and its homogeneity turn out to be over-estimated theoretically because the uniform polarizations of the tile permanent magnets generate a decrease in the homogeneity of the magnetic field.
The analytical method we use in this paper is based on the coulombian model of a magnet. This model implies the existence of fictitious magnetic charges located on the faces or in the volume of a permanent magnet [19]. Such an analytical method has been widely used by many authors for calculating the magnetic field produced by ring permanent magnets radially and axially magnetized [20][21], tile permanent magnets radially magnetized [22], tile permanent magnets uniformly magnetized [23][24].
First, this paper presents the exact three-dimensional analytical expressions that allow us to study the homogeneity and the magnitude of the magnetic field produced by an assembly of tile permanent magnets uniformly magnetized. Then, we discuss the influence of the number of tile permanent magnets used on the magnetic field properties.

## 2. MODELING THE MAGNETIC FIELD INSIDE THE MRI STRUCTURE

We propose in this section to determine the expressions of the magnetic field components in cartesian coordinates for studying the homogeneity of the field inside the MRI structure. For this purpose, let us first consider the configuration shown in Fig. 1. The eight tile permanent magnets are uniformly magnetized. The parameters used in this paper are shown in Fig 2 in which we have represented only one tile permanent magnet uniformly magnetized. We have to consider only one tile permanent magnet whose polarization is both uniform and arbitrary. Indeed, the total magnetic field produced by an assembly

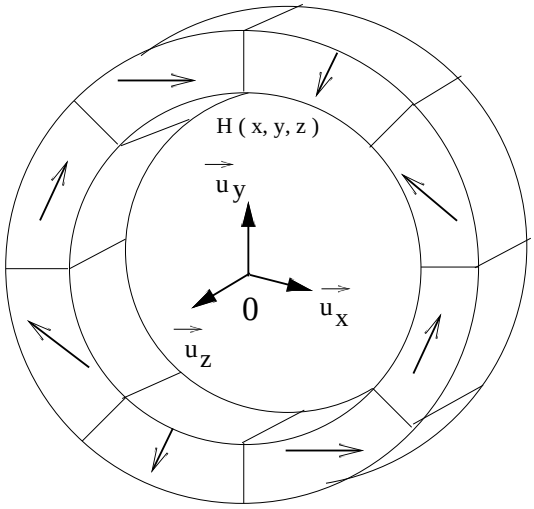


**Figure 1.** Illustration of a MRI structure with 8 tile permanent magnets uniformly magnetized

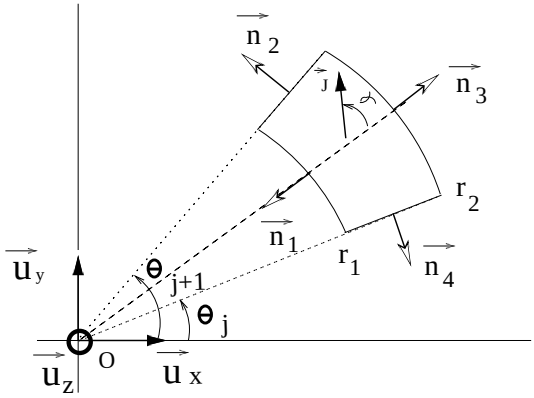


**Figure 2.** Parameters used for studying the magnetic field produced by the MRI structure

of tile permanent magnets can be obtained by using the principle of superposition.

As the tile permanent magnets are uniformly magnetized, each tile permanent magnet can be represented by fictitious magnetic pole surface densities located on its faces in the coulombian approach. By

denoting $\sigma^*_{j,i}$, the fictitious magnetic pole surface density located on the $i^{th}$ face of the magnet $j$ whose angular width equals $\theta_{j+1} - \theta_j$, the fictitious manetic pole surface densities are given by the scalar product $\vec{J}.\vec{n}_j$ where $j = 1..4$ (as shown in Fig 2). After mathematical manipulations, we find $\sigma^*_{j,1}$, $\sigma^*_{j,2}$, $\sigma^*_{j,3}$ and $\sigma^*_{j,4}$ in the following reduced forms:

$$\begin{aligned}
\sigma^*_{j,1} &= -J\cos\left(\theta - a - \frac{\theta_j + \theta_{j+1}}{2}\right) \\
\sigma^*_{j,2} &= -J\sin\left(\frac{\theta_{j+1} - \theta_j}{2} - a\right) \\
\sigma^*_{j,3} &= J\cos\left(\theta - a - \frac{\theta_j + \theta_{j+1}}{2}\right) \\
\sigma^*_{j,4} &= J\sin\left(\frac{\theta_j - \theta_{j+1}}{2} - a\right)
\end{aligned} \tag{1}$$

It is useful to define the three-dimensional Green's function as follows:

$$G_0(\vec{r}, \vec{r'}) = \frac{1}{4\pi\left|\vec{r} - \vec{r'}\right|} \tag{2}$$

where $\vec{r}$ is the observation point and $\vec{r'}$ a point located on the fictitious charge distribution. For the rest of this paper, we use the four following definitions of the three-dimensional Green's function:

$$\begin{aligned}
G_0(\vec{r}, \vec{r'})^{(1)} &= (4\pi)^{-1}\left(r_1^2 + \tilde{r}^2 - 2r_1\tilde{r}\cos(\theta - \tilde{\theta}) + (z - \tilde{z})^2\right)^{-\frac{1}{2}} \\
G_0(\vec{r}, \vec{r'})^{(2)} &= (4\pi)^{-1}\left(r^2 + \tilde{r}^2 - 2r\tilde{r}\cos(\theta - \theta_{j+1}) + (z - \tilde{z})^2\right)^{-\frac{1}{2}} \\
G_0(\vec{r}, \vec{r'})^{(3)} &= (4\pi)^{-1}\left(r_2^2 + \tilde{r}^2 - 2r_2\tilde{r}\cos(\theta - \tilde{\theta}) + (z - \tilde{z})^2\right)^{-\frac{1}{2}} \\
G_0(\vec{r}, \vec{r'})^{(4)} &= (4\pi)^{-1}\left(r^2 + \tilde{r}^2 - 2r\tilde{r}\cos(\theta - \theta_j) + (z - \tilde{z})^2\right)^{-\frac{1}{2}}
\end{aligned} \tag{3}$$

It is emphasized here that the use of the three-dimensional Green's function is absolutely equivalent to the coulombian model of a magnet because the structure considered in this paper is ironless. For a tile permanent magnet having an angular width that equals $\theta_{j+1} - \theta_j$, the $x$-component of the magnetc field is given by:

$$H_x(x, y, z) = \cos(\theta)\partial_r\left\{\sum_{k=1}^{4}\int_{S_k} G_0(\vec{r}, \vec{r'})^{(k)}\sigma^*_{j,k}(\vec{r'})d^2\vec{r'}_k\right\}$$

$$- \sin(\theta) r^{-1} \partial_\theta \left\{ \sum_{k=1}^{4} \int_{S_k} G_0(\vec{r}, \vec{r'})^{(k)} \sigma^*_{j,k}(\vec{r'}) d^2 \vec{r'}_k \right\} \tag{4}$$

The $y$-component of the magnetc field is given by:

$$\begin{aligned} H_y(x,y,z) &= \sin(\theta) \partial_r \left\{ \sum_{k=1}^{4} \int_{S_k} G_0(\vec{r}, \vec{r'})^{(k)} \sigma^*_{j,k}(\vec{r'}) d^2 \vec{r'}_k \right\} \\ &+ \cos(\theta) r^{-1} \partial_\theta \left\{ \sum_{k=1}^{4} \int_{S_k} G_0(\vec{r}, \vec{r'})^{(k)} \sigma^*_{j,k}(\vec{r'}) d^2 \vec{r'}_k \right\} \end{aligned} \tag{5}$$

The $z$-component of the magnetic field is given by:

$$H_z(x,y,z) = -\partial_z \left\{ \sum_{k=1}^{4} \int_{S_k} G_0(\vec{r}, \vec{r'})^{(k)} \sigma^*_{j,k}(\vec{r'}) d^2 \vec{r'}_k \right\} \tag{6}$$

The previous relations can be developed as follows:

$$\begin{aligned} H_x(x,y,z) &= \cos(\theta) \partial_r \left\{ \int_{\theta_j}^{\theta_{j+1}} \int_{z_1}^{z_2} G_0(\vec{r}, \vec{r'})^{(1)} \sigma^*_{j,1} r_1 d\tilde{\theta} d\tilde{z} \right\} \\ &+ \cos(\theta) \partial_r \left\{ \int_{r_1}^{r_2} \int_{z_1}^{z_2} G_0(\vec{r}, \vec{r'})^{(2)} \sigma^*_{j,2} d\tilde{r} d\tilde{z} \right\} \\ &+ \cos(\theta) \partial_r \left\{ \int_{\theta_j}^{\theta_{j+1}} \int_{z_1}^{z_2} G_0(\vec{r}, \vec{r'})^{(3)} \sigma^*_{j,3} r_2 d\tilde{\theta} d\tilde{z} \right\} \\ &+ \cos(\theta) \partial_r \left\{ \int_{r_1}^{r_2} \int_{z_1}^{z_2} G_0(\vec{r}, \vec{r'})^{(4)} \sigma^*_{j,4} d\tilde{r} d\tilde{z} \right\} \\ &- \sin(\theta) r^{-1} \partial_\theta \left\{ \int_{\theta_j}^{\theta_{j+1}} \int_{z_1}^{z_2} G_0(\vec{r}, \vec{r'})^{(1)} \sigma^*_{j,1} r_1 d\tilde{\theta} d\tilde{z} \right\} \\ &- \sin(\theta) r^{-1} \partial_\theta \left\{ \int_{r_1}^{r_2} \int_{z_1}^{z_2} G_0(\vec{r}, \vec{r'})^{(2)} \sigma^*_{j,2} d\tilde{r} d\tilde{z} \right\} \\ &- \sin(\theta) r^{-1} \partial_\theta \left\{ \int_{\theta_j}^{\theta_{j+1}} \int_{z_1}^{z_2} G_0(\vec{r}, \vec{r'})^{(3)} \sigma^*_{j,3} r_2 d\tilde{\theta} d\tilde{z} \right\} \\ &- \sin(\theta) r^{-1} \partial_\theta \left\{ \int_{r_1}^{r_2} \int_{z_1}^{z_2} G_0(\vec{r}, \vec{r'})^{(4)} \sigma^*_{j,4} d\tilde{r} d\tilde{z} \right\} \end{aligned} \tag{7}$$

$$
\begin{aligned}
H_y(x,y,z) &= \sin(\theta)\partial_r\left\{\int_{\theta_j}^{\theta_{j+1}}\int_{z_1}^{z_2} G_0(\vec{r},\vec{r'})^{(1)}\sigma^*_{j,1}r_1 d\tilde{\theta}d\tilde{z}\right\} \\
&+\sin(\theta)\partial_r\left\{\int_{r_1}^{r_2}\int_{z_1}^{z_2} G_0(\vec{r},\vec{r'})^{(2)}\sigma^*_{j,2}d\tilde{r}d\tilde{z}\right\} \\
&+\sin(\theta)\partial_r\left\{\int_{\theta_j}^{\theta_{j+1}}\int_{z_1}^{z_2} G_0(\vec{r},\vec{r'})^{(3)}\sigma^*_{j,3}r_2 d\tilde{\theta}d\tilde{z}\right\} \\
&+\sin(\theta)\partial_r\left\{\int_{r_1}^{r_2}\int_{z_1}^{z_2} G_0(\vec{r},\vec{r'})^{(4)}\sigma^*_{j,4}d\tilde{r}d\tilde{z}\right\} \\
&+\cos(\theta)r^{-1}\partial_\theta\left\{\int_{\theta_j}^{\theta_{j+1}}\int_{z_1}^{z_2} G_0(\vec{r},\vec{r'})^{(1)}\sigma^*_{j,1}r_1 d\tilde{\theta}d\tilde{z}\right\} \\
&+\cos(\theta)r^{-1}\partial_\theta\left\{\int_{r_1}^{r_2}\int_{z_1}^{z_2} G_0(\vec{r},\vec{r'})^{(2)}\sigma^*_{j,2}d\tilde{r}d\tilde{z}\right\} \\
&+\cos(\theta)r^{-1}\partial_\theta\left\{\int_{\theta_j}^{\theta_{j+1}}\int_{z_1}^{z_2} G_0(\vec{r},\vec{r'})^{(3)}\sigma^*_{j,3}r_2 d\tilde{\theta}d\tilde{z}\right\} \\
&+\cos(\theta)r^{-1}\partial_\theta\left\{\int_{r_1}^{r_2}\int_{z_1}^{z_2} G_0(\vec{r},\vec{r'})^{(4)}\sigma^*_{j,4}d\tilde{r}d\tilde{z}\right\}
\end{aligned} \tag{8}
$$

$$
\begin{aligned}
H_z(x,y,z) &= -\partial_z\left\{\int_{\theta_j}^{\theta_{j+1}}\int_{z_1}^{z_2} G_0(\vec{r},\vec{r'})^{(1)}\sigma^*_{j,1}r_1 d\tilde{\theta}d\tilde{z}\right\} \\
&-\partial_z\left\{\int_{r_1}^{r_2}\int_{z_1}^{z_2} G_0(\vec{r},\vec{r'})^{(2)}\sigma^*_{j,2}d\tilde{r}d\tilde{z}\right\} \\
&-\partial_z\left\{\int_{\theta_j}^{\theta_{j+1}}\int_{z_1}^{z_2} G_0(\vec{r},\vec{r'})^{(3)}\sigma^*_{j,3}r_2 d\tilde{\theta}d\tilde{z}\right\} \\
&-\partial_z\left\{\int_{r_1}^{r_2}\int_{z_1}^{z_2} G_0(\vec{r},\vec{r'})^{(4)}\sigma^*_{j,4}d\tilde{r}d\tilde{z}\right\}
\end{aligned} \tag{9}
$$

After mathematical manipulations, $H_x(x,y,z)$, $H_y(x,y,z)$ and $H_z(x,y,z)$ can be written as follows:

$$
\begin{aligned}
H_x(x,y,z) &= \frac{J\cos(\theta)}{4\pi\mu_0}\left(\sin\left(\frac{\theta_j-\theta_{j+1}}{2}+\alpha\right)f(\theta_j)+\sin\left(\frac{\theta_j-\theta_{j+1}}{2}-\alpha\right)f(\theta_{j+1})\right) \\
&+\frac{J\cos(\theta)}{4\pi\mu_0}\sum_{i=1}^{2}\sum_{k=1}^{2}(-1)^{(i+k)}r_i(-z+z_k)\mathbf{N}[\tilde{\theta}]
\end{aligned}
$$

$$-\frac{J\sin(\theta)}{4\pi\mu_0}\left\{\sin\left(\frac{\theta_j-\theta_{j+1}}{2}-\alpha\right)h(\theta_j)+\sin\left(\frac{\theta_j-\theta_{j+1}}{2}+\alpha\right)h(\theta_{j+1})\right\}$$
$$-\frac{J\sin(\theta)}{4\pi\mu_0}\int_{\theta_j}^{\theta_{j+1}}\sum_{i=1}^{2}\sum_{k=1}^{2}\frac{r_i^2(-z+z_k)\cos\left(\alpha+\frac{\theta_j-\theta_{j+1}}{2}-\tilde{\theta}\right)\sin(\theta-\tilde{\theta})}{(r^2+r_i^2-2rr_i\cos(\theta-\tilde{\theta}))\epsilon(\tilde{\theta})}d\tilde{\theta} \tag{10}$$

$$\begin{aligned}H_y(x,y,z) &= \frac{J\sin(\theta)}{4\pi\mu_0}\left(\sin\left(\frac{\theta_j-\theta_{j+1}}{2}+\alpha\right)f(\theta_j)+\sin\left(\frac{\theta_j-\theta_{j+1}}{2}-\alpha\right)f(\theta_{j+1})\right)\\ &+\frac{J\sin(\theta)}{4\pi\mu_0}\sum_{i=1}^{2}\sum_{k=1}^{2}(-1)^{(i+k)}r_i(-z+z_k)\mathbf{N}[\tilde{\theta}]\\ &+\frac{J\cos(\theta)}{4\pi\mu_0}\left\{\sin\left(\frac{\theta_j-\theta_{j+1}}{2}-\alpha\right)h(\theta_j)+\sin\left(\frac{\theta_j-\theta_{j+1}}{2}+\alpha\right)h(\theta_{j+1})\right\}\\ &+\frac{J\cos(\theta)}{4\pi\mu_0}\int_{\theta_j}^{\theta_{j+1}}\sum_{i=1}^{2}\sum_{k=1}^{2}\frac{r_i^2(-z+z_k)\cos\left(\alpha+\frac{\theta_j-\theta_{j+1}}{2}-\tilde{\theta}\right)\sin(\theta-\tilde{\theta})}{(r^2+r_i^2-2rr_i\cos(\theta-\tilde{\theta}))\epsilon(\tilde{\theta})}d\tilde{\theta}\end{aligned} \tag{11}$$

$$\begin{aligned}H_z(x,y,z) &= \frac{J}{4\pi\mu_0}\left(\sin\left(\frac{\theta_1-\theta_2}{2}-\alpha\right)g(\theta_2)+\sin\left(\frac{\theta_1-\theta_2}{2}+\alpha\right)g(\theta_1)\right)\\ &+\frac{J}{4\pi\mu_0}\int_{\theta_1}^{\theta_2}\sum_{i=1}^{2}\sum_{k=1}^{2}\frac{r_i\cos(\alpha+\frac{\theta_1-\theta_2}{2}-\tilde{\theta})}{\epsilon(\theta_j)}d\tilde{\theta}\end{aligned} \tag{12}$$

with

$$\begin{aligned}g(\theta_j) &= \sum_{i=1}^{2}\sum_{k=1}^{2}\log\left[r_i-r\cos(\theta-\theta_j)+\epsilon(\theta_j)\right]\\ f(\theta_j) &= \sum_{i=1}^{2}\sum_{k=1}^{2}(-1)^{(i+k)}\left(-\cos(\theta-\theta_j)\log[X_j]+\sin(\theta-\theta_j)\arctan[Y_j]\right)\\ h(\theta_j) &= \sum_{i=1}^{2}\sum_{k=1}^{2}\sin(\theta-\theta_j)\log\left[X_j\right]-\cos(\theta-\theta_j)\arctan\left[Y_j\right]\end{aligned} \tag{13}$$

$$\mathbf{N}[\tilde{\theta}]=\int_{\theta_j}^{\theta_{j+1}}\frac{\left(r-r_i\cos(\theta-\tilde{\theta})\right)\cos(\alpha+\frac{\theta_j-\theta_{j+1}}{2}-\tilde{\theta})}{\left(r^2+r_i^2-2rr_i\cos(\theta-\tilde{\theta})\right)\epsilon(\tilde{\theta})}d\tilde{\theta} \tag{14}$$

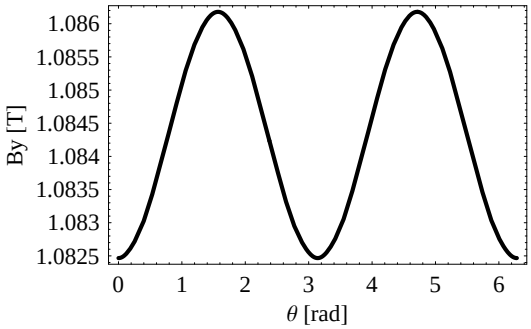


**Figure 3.** Representation of the $y$-component of the magnetic field versus the angle $\theta$ for 16 tile permanent magnets: we take the following dimensions: $r_1 = 0.3$ m, $r_2 = 0.6$ m, $z_1 = 0$ m, $z_2 = 1.6$ m, $z = 0.8$ m, $J = 1.5$ T, $r = \frac{r_1}{2}$.

$$\begin{aligned} X_j &= z - z_k + \epsilon(\theta_j) \\ Y_j &= \frac{(z - z_k)\,(r_i - r\cos(\theta - \theta_j))}{r\sin(\theta - \theta_j)\epsilon(\theta_j)} \\ \epsilon(\beta) &= \sqrt{r^2 + r_i^2 + (z - z_k)^2 - 2rr_i\cos(\theta - \beta)} \end{aligned} \tag{15}$$

We represent in Fig 3 the $y$-component of the magnetic field versus the angle $\theta$ and in Fig 4 the $x$-component of the magnetic field versus $\theta$. Figures 3 and 4 show that there is a undulation of the magnetic field that comes from the uniform polarizations of the tile permanent magnets.

### 2.1. The end effects on the magnetic field value

The homogeneity of the magnetic field depends also on the length of the Magnetic Resonance Imaging structure. For example, the finite dimensions along the $z$-direction (axial direction) generates a curvature in the field, as shown in Fig 5. Indeed, the magnetic lines are less and less packed together near the edges ($z = 0$ m and $z = 1.6$ m). Consequently, this implies a decrease in the $y$-field magnitude when the observation point is determined far from the middle ($z = 0.8$ m) of the MRI structure.

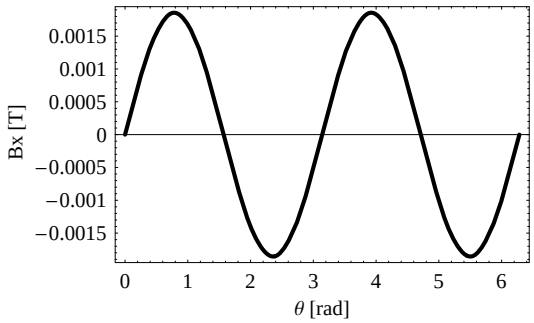


**Figure 4.** Representation of the $x$-component of the magnetic field versus the angle $\theta$ for 16 tile permanent magnets: we take the following dimensions: $r_1 = 0.3$ m, $r_2 = 0.6$ m, $z_1 = 0$ m, $z_2 = 1.6$ m, $z = 0.8$ m, $J = 1.5$ T, $r = \frac{r_1}{2}$.

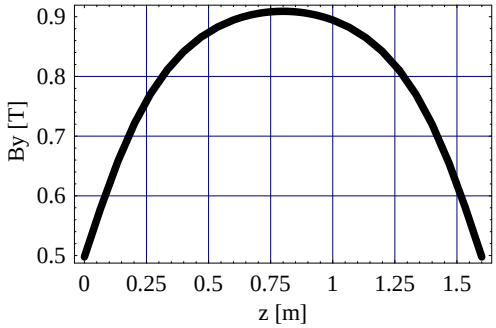


**Figure 5.** Representation of By versus $z$ with 16 tile permanent magnets: we take the following dimensions: $r_1 = 0.3$ m, $r_2 = 0.6$ m, $z_1 = 0$ m, $z_2 = 1.6$ m, $z = 0.8$ m, $J = 1.5$ T, $r = 0$ m.

## 2.2. Influence of the outer radius on the magnetic field magnitude

Another important parameter that can be used for enhancing the magnetic field value is the outer radius. As shown in Fig 6, the more important the outer radius is, the greater the magnetic field value is. Consequently, despite the expensive cost of permanent magnets, this implies that for a given inner radius $r_{in}$, the value of the outer radius $r_{out}$ must be the greatest.

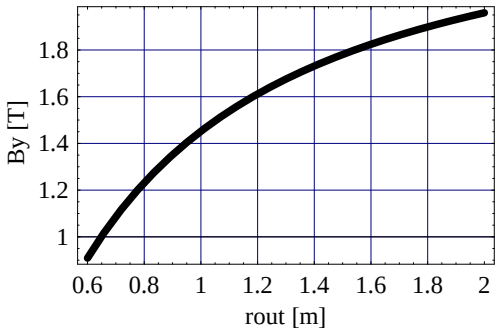


**Figure 6.** Representation of By versus $r_{out}$ [m] with 16 tile permanent magnets: we take the following dimensions: $r_1 = 0.3$ m, $z_1 = 0$ m, $z_2 = 1.6$ m, $z = 0.8$ m, $J = 1.5$ T, $r = 0$ m.

## 3. INFLUENCE OF THE NUMBER OF TILE PERMANENT MAGNETS ON THE FIELD PROPERTIES

### 3.1. Influence of the number of tile permanent magnets on the field value

This section presents the influence of the number of tile permanent magnets on the field value. Strictly speaking, we take the mean value of the magnetic field on a radial length that equals $r = \frac{r_1}{2}$. We take the following dimensions: $r_1 = 0.3$ m, $r_2 = 0.6$ m, $z_1 = 0$ m, $z_2 = 1.6$ m, $z = 0.8$ m, $J = 1.5$ T. Furthermore, the angular width $\Delta\theta$ of each tile permanent magnet is the same and is given by the number of tile permanent magnets used.

$$\Delta\theta = \theta_{j+1} - \theta_j = \frac{N}{2\pi} \tag{16}$$

where $N$ is the number of tile permanent magnets used in the structure. We represent in Fig 7 the mean value of the magnetic field $< B >= B_y = \mu_0 H_y$ versus the number of tile permanent magnets used. Figure 7 clearly shows that the greater the number of tile permanent magnets is, the higer the magnetic field is. However, according to this criterion, the evolution of the increase in magnetic field value is not constant but decreases with the number of tile permanent magnets used.

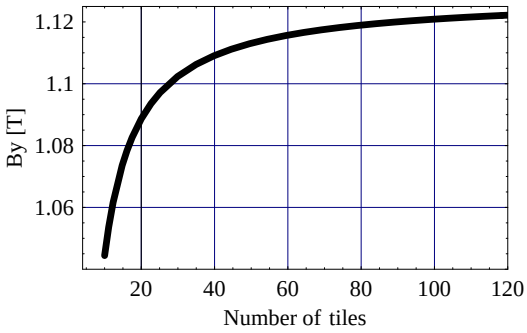


**Figure 7.** Representation of the magnetic field $By$ versus the number of tile permanent magnets used: we take the following dimensions: $r_1 = 0.3$ m, $r_2 = 0.6$ m, $z_1 = 0$ m, $z_2 = 1.6$ m, $z = 0.8$ m, $J = 1.5$ T, $r = \frac{r_1}{2}$.

### 3.2. Influence of the number of tile permanent magnets on the field homogeneity

This section presents the influence of the number of tile permanent magnets on the field homogeneity. For this purpose, we define the concept of wave rate $WR$ as follows:

$$WR = \frac{1}{2}\frac{B_{max} - B_{min}}{B_{moy}} \tag{17}$$

where $B_{max}$ and $B_{min}$ are the maximum minimum values of the magnetic field, $B_{moy}$ is the mean value of the magnetic field. According to this criterion, the weaker the wave rate is, the greater the magnetic field homogeneity is. Let us study the influence of the number $N$ of tile permanent magnets on the wave rate. For this purpose, we represent the wave rate versus N in Fig 8. Figure 8 shows that the wave rate is constant when we use at least 16 tile permanent magnets. Consequently, it is not necessary to use further tile permanent magnets for enhancing the magnetic field homogeneity in the MRI structure with the dimensions taken in this paper.

### 3.3. Two-dimensional representation of the magnetic field magnitude for two axial observation points

We illustrate now the use of our three-dimensional analytical expressions with the 2D representation of the magnetic field for eight radial observation points ($r = 0.029$ m, $r = 0.027$ m, $r = 0.025$ m,

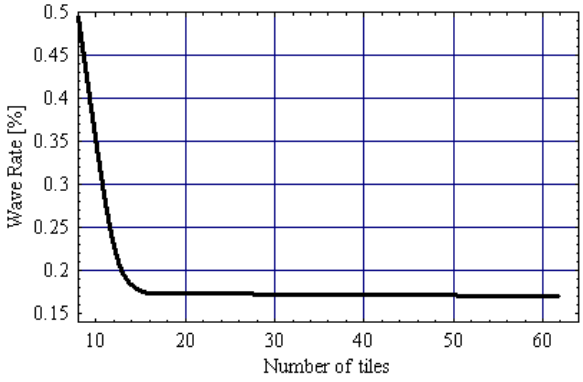


**Figure 8.** Representation of the wave rate of the magnetic field versus the number of tile permanent magnets used: we take the following dimensions: $r_1 = 0.3$ m, $r_2 = 0.6$ m, $z_1 = 0$ m, $z_2 = 1.6$ m, $z = 0.8$ m, $J = 1.5$ T, $r = \frac{r_1}{2}$.

$r = 0.023$ m, $r = 0.021$ m, $r = 0.019$ m, $r = 0.017$ m, $r = 0.015$ m) at a given axial observation point ($z = 0.08$ m). These eight representations are shown in Figs 9. The MRI structure we consider is composed of eight tile permanent magnets uniformly magnetized.

Figure 9 clearly shows that the magnetic field undulation is the greatest near the structure, that is, when $r = 0.029$ m. This undulation wave decreases when the radial observation point goes away from $r_1$. Such illustrations give elements of information about the homogeneity of the magnetic field in the MRI structure. Consequently, it gives indications about the region in space in which the magnetic field undulation is weak.

## 4. CONCLUSION

This paper has presented exact three-dimensional analytical expressions for studying the magnetic field produced by a MRI structure. These expressions are useful because all the effects due to the uniform polarizations of the tile permanent magnets are taken into account. We have demonstrated that the number of tile permanent magnets used has a great importance on the field value and its homogeneity. For example, with the dimensions taken in this paper, we have seen that the use of at least 20 tile permanent magnets allow one to obtain a high magnetic field. On the other hand, we have shown that the wave rate is not improved when we use at least 16 tile permanent magnets. Fur-

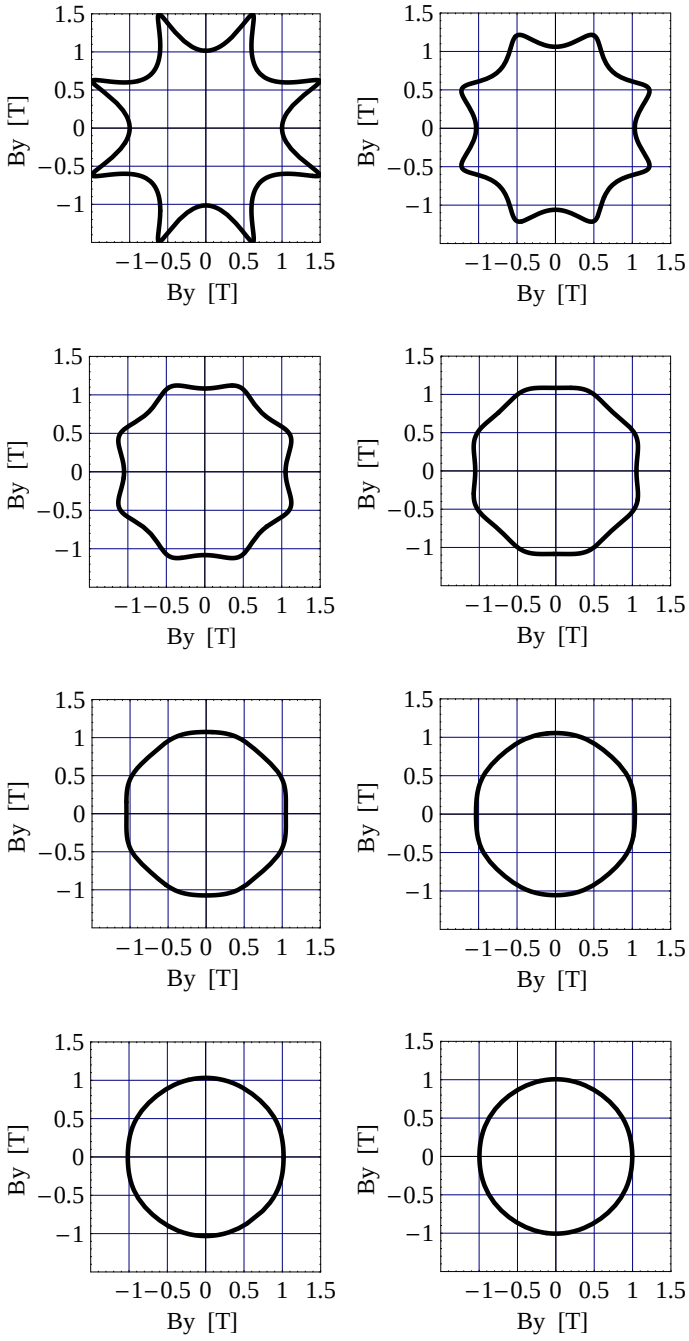


**Figure 9.** Representation of the magnetic field for 8 radial observation points ($r = 0.029$ m, $r = 0.027$ m, $r = 0.025$ m, $r = 0.023$ m, $r = 0.021$ m, $r = 0.019$ m, $r = 0.017$ m, $r = 0.015$ m)at a given axial observation point ($z = 0.08$ m): we take the following dimensions: $r_1 = 0.3$ m, $r_2 = 0.6$ m, $z_1 = 0$ m, $z_2 = 1.6$ m, $J = 1.5$ T.

thermore, we have discussed the interest of using permanent magnets with great outer radius. Indeed, this allows us to improve significantly the magnetic field magnitude inside the MRI structure.

## REFERENCES


1. A. E. Marble, "Strong, stray static magnetic fields," *IEEE Trans. Magn.*, vol. 44, no. 5, pp. 576–580, 2008.
2. W. Chang, K. Chen, and L. Hwang, "Single-sided mobile nmr with a halbach magnet," *Magnetic Resonance Imaging*, vol. 24, no. 8, pp. 1095–1102, 2006.
3. H. A. Leupold, E. P. II, and M. G. Abele, "Applications of yokeless flux confinement," *J. Appl. Phys.*, vol. 64, no. 3, 1988.
4. J. Chen and C. Xu, "An improved discrete configuration of a cylinder magnet for portable nuclear magnetic resonance instruments," *J. Appl. Phys.*, vol. 101, no. 12, 2007.
5. Z. Ren, D. Xie, and H. Li, "Study on shimming method for open permanent magnet of mri," *Progress in Electromagnetics Research M*, vol. 6, pp. 23–34, 2009.
6. T. Shirai, T. Haishi, S. Utsuzawa, Y. Matsuda, and K. Kose, "Development of a compact mouse mri using a yokeless permanent magnet," *Magnetic Resonance in Medical Sciences*, vol. 4, no. 3, pp. 137–143, 2005.
7. M. Abele and H. A. Leupold, "A general method for flux confinement in permanent magnet structure," *J. Appl. Phys.*, vol. 64, no. 10, pp. 5988–5990, 1988.
8. M. Abele, J. Jensen, and H. Rusinek, "Generation of uniform high fields with magnetized wedges," *IEEE Trans. Magn.*, vol. 33, no. 5, pp. 3874–3876, 1997.
9. C. Li and M. Devine, "Efficiency of permanent magnet assemblies for mri devices," *IEEE Trans. Magn.*, vol. 41, no. 10, pp. 3835–3837, 2005.
10. K. Miyata, K. Ohashi, A. Muraoka, and N. Takahashi, "3-d magnetic field analysis of permanent-magnet type of mri taking account of minor loop," *IEEE Trans. Magn.*, vol. 42, no. 4, pp. 1451–1454, 2006.
11. A. Podol'skii, "Development of permanent magnet assembly for mri devices," *IEEE Trans. Magn.*, vol. 34, no. 1, pp. 248–252, 1998.
12. A. E. Marble, I. V. Mastikhui, B. G. Colpitts, and B. J. Balcom, "Designing static fields for unilateral magnetic resonance by a

scalar potential approach," *IEEE Trans. Magn.*, vol. 43, no. 5, pp. 1903–1911, 2007.

13. J. S. Ryu, Y. Yao, C. S. Koh, and Y. J. Shin, "Development of permanent magnet assembly for mri devices," *IEEE Trans. Magn.*, vol. 42, no. 4, pp. 1351–1353, 2006.
14. N. Takahashi, A. Muraoka, D. Miyagi, K. Miyata, and K. Okashi, "3-d fem analysis of residual magnetism produced by x-gradient coil of permanent magnet type of mri," *IEEE Trans. Magn.*, vol. 43, no. 4, pp. 1809–1812, 2007.
15. G. Sinha, R. Sandararaman, and G. Singh, "Design concepts of optimized mri magnet," *IEEE Trans. Magn.*, vol. 44, no. 10, pp. 2351–2360, 2008.
16. M. R. Thompson, R. W. Brown, and V. C. Srivastava, "An inverse approach to the design of mri main magnets," *IEEE Trans. Magn.*, vol. 30, no. 1, pp. 108–112, 1994.
17. K. Halbach, "Strong rare earth cobalt quadrupoles," *IEEE Trans. Magn.*, vol. 26, no. 3, pp. 3882–3884, 1979.
18. R. Ravaud and G. Lemarquand, "Discussion about the magnetic field produced by cylindrical halbach structures," *Progress in Electromagnetics Research B*, vol. 13, pp. 275–308, 2009.
19. S. I. Babic, C. Akyel, and M. M. Gavrilovic, "Calculation improvement of 3d linear magnetostatic field based on fictitious magnetic surface charge," *IEEE Trans. Magn.*, vol. 36, no. 5, pp. 3125–3127, 2000.
20. R. Ravaud, G. Lemarquand, V. Lemarquand, and C. Depollier, "Analytical calculation of the magnetic field created by permanent-magnet rings," *IEEE Trans. Magn.*, vol. 44, no. 8, pp. 1982–1989, 2008.
21. R. Ravaud, G. Lemarquand, V. Lemarquand, and C. Depollier, "Discussion about the analytical calculation of the magnetic field created by permanent magnets.," *Progress in Electromagnetics Research B*, vol. 11, pp. 281–297, 2009.
22. R. Ravaud, G. Lemarquand, V. Lemarquand, and C. Depollier, "The three exact components of the magnetic field created by a radially magnetized tile permanent magnet.," *Progress in Electromagnetics Research, PIER 88*, pp. 307–319, 2008.
23. R. Ravaud and G. Lemarquand, "Analytical expression of the magnetic field created by tile permanent magnets tangentially magnetized and radial currents in massive disks," *Progress in Electromagnetics Research B*, vol. 13, pp. 309–328, 2009.
24. R. Ravaud, G. Lemarquand, V. Lemarquand, and C. Depollier,

"Magnetic field produced by a tile permanent magnet whose polarization is both uniform and tangential," *Progress in Electromagnetics Research B*, vol. 13, pp. 1–20, 2009.